Laser Chem., 1998, Vol. 17, pp. 219–237
Reprints available directly from the publisher
Photocopying permitted by license only

KINETIC STUDY OF THE REACTION OF Rh($a^4F_{9/2}$) WITH N_2O, O_2 AND NO

MARK L. CAMPBELL*

Chemistry Department, United States Naval Academy, Annapolis, MD 21402 USA

(Received 21 January 1998)

The gas phase reactivity of Rh($a^4F_{9/2}$) with N_2O, O_2 and NO is reported. Removal rate constants for the excited states of rhodium below 13,000 cm^{-1} are also reported. The reaction rate of Rh($a^4F_{9/2}$) with N_2O is relatively temperature insensitive. The rate constants for the bimolecular reaction are described in Arrhenius form by $(1.3 \pm 0.3) \times 10^{-12} \exp(-1.3 \pm 0.8\,kJ/mol/RT)\,cm^3\,s^{-1}$. The reaction rates of the $a^4F_{9/2}$ state with O_2 and NO are pressure dependent. For O_2, the limiting low-pressure third-order, k_0, and limiting high-pressure second-order, k_∞, room temperature rate constants in argon buffer are $(6.6 \pm 0.6) \times 10^{-30}\,cm^6\,s^{-1}$ and $(2.1 \pm 0.2) \times 10^{-11}\,cm^3\,s^{-1}$, respectively. For NO, k_0 and k_∞ are $(1.3 \pm 0.2) \times 10^{-30}\,cm^6\,s^{-1}$ and $(1.2 \pm 0.4) \times 10^{-11}\,cm^3\,s^{-1}$, respectively. The removal rates of the excited states are faster than the ground state by a factor of 2 or more.

Keywords: Rhodium; kinetics; gas-phase; N_2O; O_2; NO

INTRODUCTION

The gas-phase chemistry of transition metal (TM) atoms in oxidation reactions has recently received considerable attention [1–30]. TM chemistry is an intriguing field of study due to the high multiplicities of the atomic ground states and the large number of low-lying metastable states. For the reactions studied thus far, the electronic state of the reactant has been observed to be an important factor in TM reactions. For example, for both the abstraction and termolecular association channels with O_2, TMs with s^1d^{n-1} configurations

* Henry Dreyfus Teacher–Scholar.

have generally been found to be more reactive than their s^2d^{n-2} counterparts [6, 12, 27].

Here we report a gas phase kinetic study of the ground $a^4F_{9/2}$ and low-lying states of rhodium with nitrous oxide, oxygen and nitric oxide. The only other kinetic studies involving gas-phase rhodium reported the reactions of ground state rhodium with small hydrocarbons [31, 32]. We are unaware of any previous kinetic studies involving oxygen-containing oxidants. The increase in the database of TM reactions will help in the interpretation of the factors affecting TM chemistry. We hope these new kinetic results will inspire further theoretical work in an effort to gain a better understanding of these reactions. Furthermore, a thorough understanding of the reactions of rhodium are important due to the significant role rhodium plays in many catalytic processes [33].

EXPERIMENTAL

Pseudo-first order kinetic experiments ([Rh] $\ll$ [oxidant]) were carried out in an apparatus with slowly flowing gas using a laser photolysis/laser-induced fluorescence (LIF) technique. The experimental apparatus and technique have been described in detail elsewhere [16]. Briefly, the reaction chamber is a stainless steel reducing 4-way cross with attached side arms and a sapphire window for optical viewing. The reaction chamber is enclosed within a convection oven (Blue M, model 206 F) for temperature dependence experiments.

Rhodium atoms in the ground and low-lying excited states below 13,000 cm^{-1} were produced by the 248 nm photodissociation of dicarbonylacetylacenato rhodium(I) [$Rh(CO)_2(acac)$] utilizing the output of an excimer laser (Lambda Physics Lextra 200). Rhodium atoms were detected *via* LIF using an excimer-pumped dye laser (Lambda Physics Lextra 50/ScanMate 2E). Transition wavelengths were taken from Duquette *et al.* [34]. The fluorescence was detected at 90° to the counterpropagated laser beams with a three-lens telescope imaged through an iris. A photomultiplier tube (Hamamatsu R375) was used in collecting the LIF which was subsequently sent to a gated boxcar sampling module (Stanford Research Systems SR250), and the digitized output was stored and analyzed by a computer.

Vapor from the $[Rh(CO)_2(acac)]$ precursor was entrained in a flow of argon buffer gas. The diluted precursor vapor, buffer gas, and reactant gas flowed through calibrated mass flow meters and flow controllers prior to admission to the reaction chamber. Each sidearm window was purged with a slow flow of argon to prevent deposition of rhodium and other photoproducts. Total flows for these experiments were between 200 and 5600 sccm. Most experiments had a flow of approximately 500 sccm. Pressures were measured with MKS Baratron manometers, and chamber temperatures were measured with a thermocouple.

The delay time between the photolysis pulse and the dye-laser pulse was varied by a digital delay generator (Stanford Research Systems DG535) controlled by a computer. The trigger source for these experiments was scattered pump laser light incident upon a fast photodiode. LIF decay traces consisted of 200 points, each point averaged for 4 laser shots.

Materials: Dicarbonylacetylacetonato rhodium(I) (Strem, 99%), O_2 (MG Industries, 99.8%), N_2O (MG Industries, electronic grade, 99.999%), N_2 (Potomac Airgas, Inc., 99.998%) and Ar (Potomac Airgas, Inc., 99.998%) were used as received. The NO (Liquid Carbonic, 99%) was passed through a liquid nitrogen/*n*-pentane trap at approximately $-100°C$ to condense impurities (primarily NO_2) before entrance into the reaction chamber.

DATA ANALYSIS AND RESULTS

The primary focus of this study was on the $a^4F_{9/2}$ ground state; however, the other low-lying excited states were also studied in order to determine the effect on the temporal decay profiles of the ground state due to physical quenching of these higher energy states. Rhodium atoms in states with less than $13{,}000\,cm^{-1}$ of electronic energy were observed under these experimental conditions. These low-lying excited electronic states were produced in a non-Boltzmann distribution immediately following the photolysis event; however, measurements of the relative populations of these states were not undertaken.

When monitoring the kinetics of the ground state, the output of the photolysis excimer was unfocused. When the excited states were

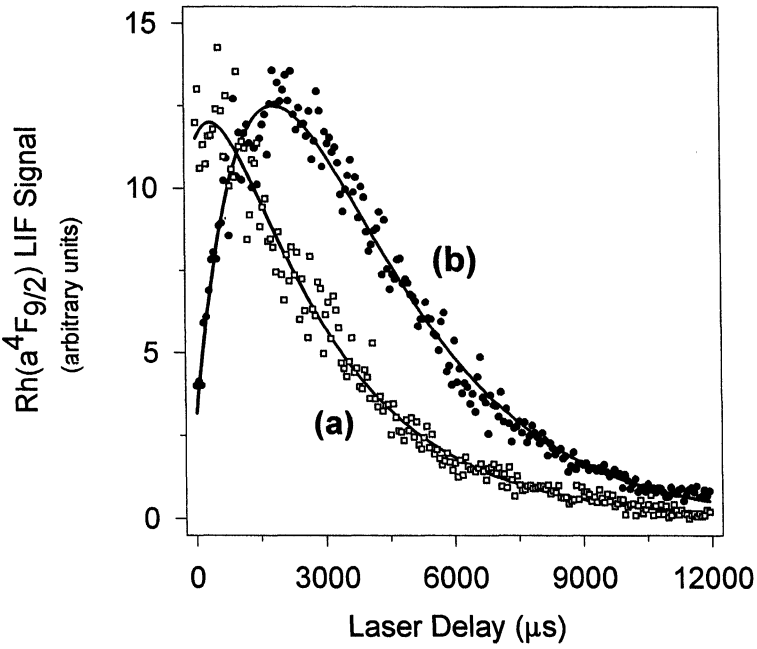

FIGURE 1 Temporal profiles for $Rh(a^4F_{9/2})$ in the absence of oxidant at 296 K and a total pressure of 20 Torr (argon buffer) with the photolysis excimer (a) unfocused and (b) focused. The solid lines are fits to Eq. (2) with (a) $\tau_1 = 670\,\mu s$, $\tau_2 = 2610\,\mu s$ and $[Rh(a^4F_{9/2})]/[Rh^*] = 2.2$ and (b) $\tau_1 = 1750\,\mu s$, $\tau_2 = 2320\,\mu s$ and $[Rh(a^4F_{9/2})]/Rh^* = 0.12$. The PMT voltages for profiles (a) and (b) are 1300 V and 1100 V, respectively.

temperature and total pressure. The majority of decay profiles showed growth (*i.e.*, nonexponential behavior) at the beginning of the decays. Again, this behavior is due to the relaxation of the excited states to the ground state. Once the excited states have relaxed to the ground state, the loss of ground state rhodium is described by the first-order decay constant, k_1:

$$k_1 = 1/\tau = k_0 + k_2[\text{oxid}] \tag{3}$$

where τ is the first-order time constant for the removal of rhodium under the given experimental conditions, k_0 is the loss term due to diffusion out of the detection zone and reaction with the precursor and precursor fragments, and k_2 is the second-order rate constant. Time

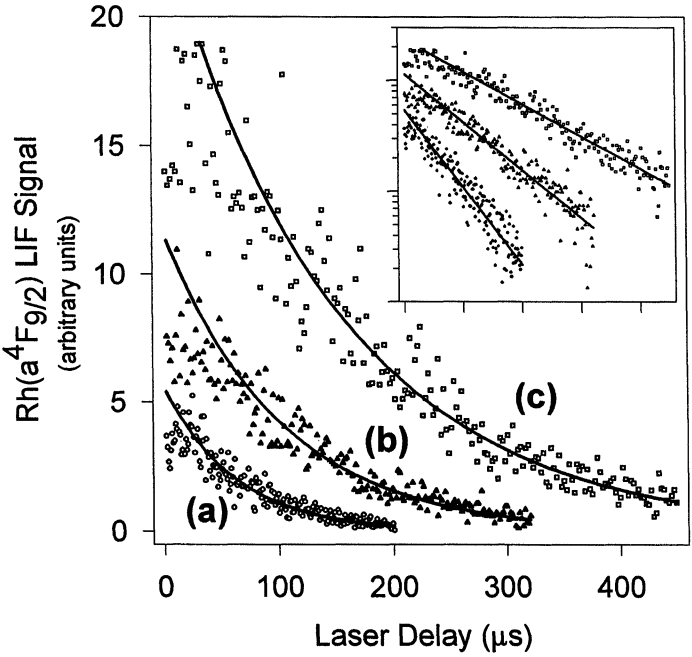

FIGURE 2 Typical $Rh(a^4F_{9/2})$ decay curves with added oxidant. The solid lines through the data are exponential fits. (a) P(NO) = 0.21 Torr, P_{total} = 75 Torr, T = 295 K, τ = 61.9 μs; (b) $P(O_2)$ = 0.041 Torr, P_{total} = 50 Torr, T = 296 K, τ = 100 μs; (c) $P(N_2O)$ = 0.33 Torr, P_{total} = 20 Torr, T = 398 K, τ = 149 μs. The inset is a ln plot of the data.

constants were determined by adjusting the range of the linear regression analysis; *i.e.*, the range did not include the beginning of the decay when growth was present. Typical decays were analyzed after a delay of approximately one reaction lifetime and included data for a length of two to three reaction lifetimes. In Figure 2 the lines through the data are exponential fits from which the pseudo-first order rate constant, $1/\tau$, is obtained.

Second-order rate constants are determined from plots of $1/\tau$ *vs.* reactant number density. Typical plots for obtaining second-order rate constants are presented in Figure 3; the slope yields the observed rate constant. The relative uncertainty (*i.e.*, the reproducibility) of the second-order rate constants is estimated at ±20%. The absolute uncertainties are estimated to be ±30% and are based on the sum of

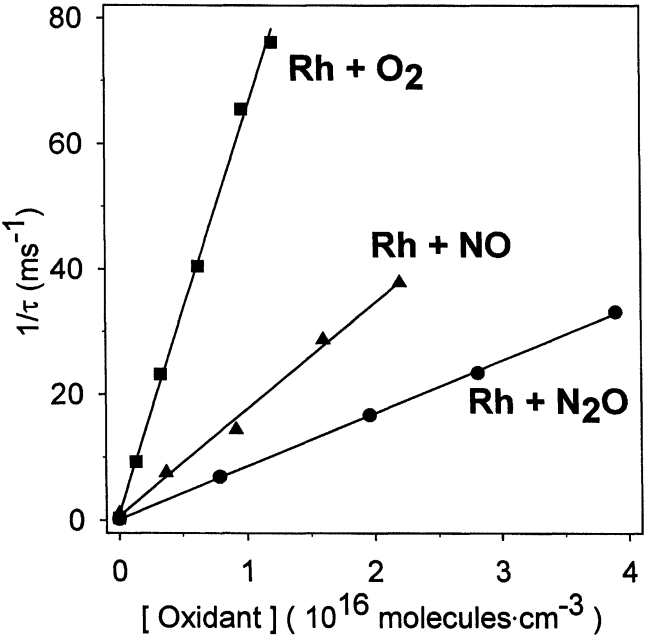

FIGURE 3 Typical plots for determining k_{2nd} for Rh($a^4F_{9/2}$). (a) Rh + O_2, P_{total} = 50 Torr, T = 296 K; (b) Rh + NO, P_{total} = 50 Torr, T = 296 K; (c) Rh + N_2O, P_{total} = 20 Torr, T = 398 K. The solid line for each set of data is a linear regression fit from which k_{2nd} is obtained.

the statistical scatter in the data and uncertainty in the flow controller and flowmeter readings (5%) and the total pressure reading (1%), uncertainties due to incomplete mixing, and uncertainties due to incomplete relaxation of the excited electronic states to the ground state.

Rh($a^4F_{9/2}$) + N_2O

Measured rate constants for the $a^4F_{9/2}$ state reacting with N_2O at various temperatures are listed in Table I. The maximum temperature attainable in this study was 548 K due to the decomposition of the precursor above this temperature. The room temperature rate constant was measured at 10, 20 and 50 Torr and is independent of total pressure within experimental uncertainty; thus, termolecular processes

TABLE I Second-order rate constants ($/10^{-13}$) for Rh($a^4F_{9/2}$) + N_2O

Temperature (*K*)	*Bimolecular rate constant* (*molecule*$^{-1}$ *cm*^{3} *s*$^{-1}$, $/10^{-13}$)
296	7.3
348	8.5
373	8.0
398	8.4
423	9.5
448	8.6
473	9.4
498	8.1
523	9.9
548	10.0

are unimportant for this reaction. The rate constants are relatively temperature insensitive indicating a small activation energy for the reaction. The rate constants are described in Arrhenius form by $(1.3 \pm 0.3) \times 10^{-12} \exp(-1.3 \pm 0.8\,\text{kJ/mol/RT})$ molecule^{-1} cm^3 s^{-1} where the uncertainties are $\pm 2\sigma$. An Arrhenius plot (ln k *vs.* $1/T$) for the $a^4F_{9/2}$ state is shown in Figure 4.

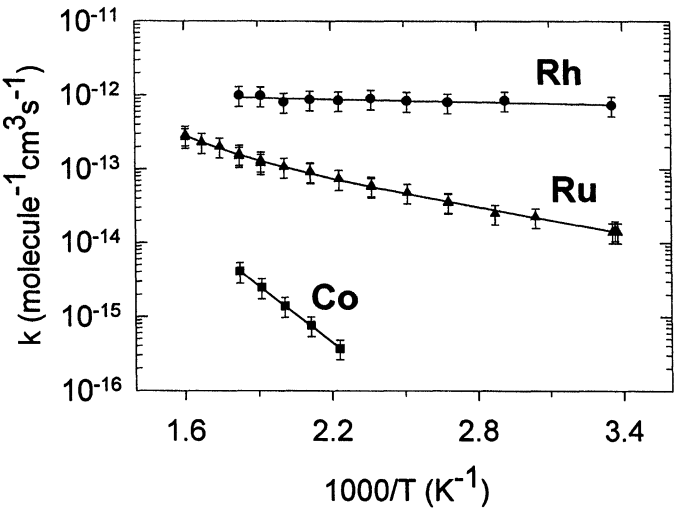

FIGURE 4 Arrhenius plot for the collisional disappearance of Rh($a^4F_{9/2}$), Co($a^4F_{9/2}$) and Ru(a^5F_5) with N_2O. Error bars represent $\pm 30\%$ uncertainty. Data for cobalt and ruthenium are from Refs. [20] and [40], respectively.

$Rh(a^4F_{9/2}) + O_2$, NO

Measured rate constants for the $a^4F_{9/2}$ state reacting with O_2 and NO in argon buffer at various pressures are listed in Table II. The rate constants at 473 K and 20 Torr for O_2 and NO are 1.8×10^{-12} and 3.0×10^{-13} molecule^{-1} cm^3 s^{-1}, respectively. These rate constants are lower than the room temperature rate constants at this pressure. Thus, for both reactions, the rate constants are dependent on total pressure and decrease with increasing temperature. The pressure dependence indicates termolecular processes for these reactants while the temperature results indicate either small or no barriers to reaction. The variation with total pressure of the second-order rate constants at room temperature in Ar buffer for O_2 and NO are shown in Figures 5 and 6, respectively. The solid lines through the data are fits to the simplified Lindemann-Hinshelwood expression [35]:

$$k = \frac{k_0[\mathrm{Ar}]}{1 + k_0[\mathrm{Ar}]/k_\infty} \tag{4}$$

where k_0 is the limiting low-pressure third-order the constant, k_∞ is the limiting high-pressure second-order rate constant, and [Ar] is the buffer gas number density. The values for k_0 and k_∞ for the reaction of

TABLE II Second-order rate constants ($/10^{-12}$) for $Rh(a^4F_{9/2}) + O_2$ and NO in Argon

Total Pressure (Torr)	k_{2nd} (*molecule*$^{-1}$ *cm*^{3} *s*$^{-1}$, 10^{-12})	
	O_2	*NO*
2.5	0.76	0.21
5	1.1	0.30
10	2.2	0.51
15	3.3	–
20	3.6	0.92
30	4.7	–
40	5.8	–
50	6.4	1.7
60	7.5	–
75	9.5	2.3
100	11.0	3.0
125	11.0	–
150	13.0	4.0
200	14.0	5.1
300	16.0	6.4

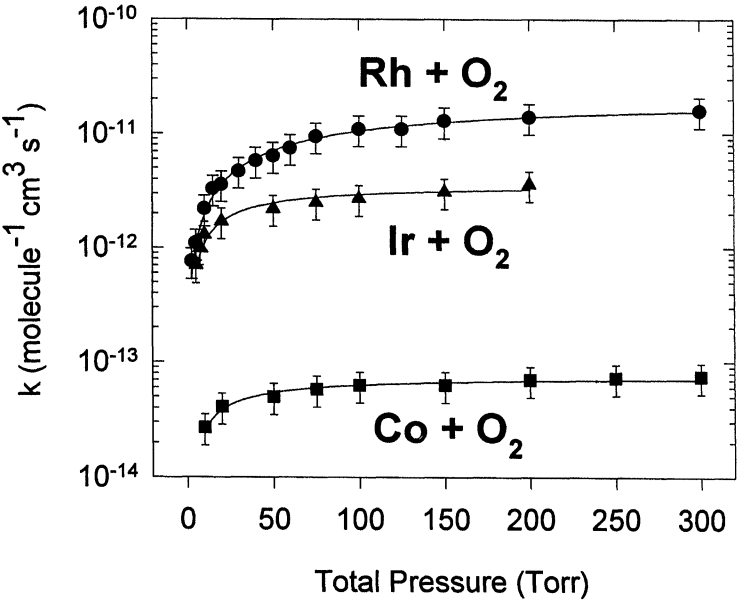

FIGURE 5 Rate constants for the reaction of ground state rhodium, cobalt and iridium + O_2 at room temperature. Error bars represent ±30% uncertainty. The solid lines are fits to Eq. (4).

O_2 in argon buffer at 296 K are $(6.6 \pm 0.6) \times 10^{-30}$ molecule^{-2} cm^6 s^{-1} and $(2.1 \pm 0.2) \times 10^{-11}$ molecule^{-1} cm^3 s^{-1}, respectively. The values for k_0 and k_∞ for the reaction of NO in argon buffer at 296 K are $(1.3 \pm 0.2) \times 10^{-31}$ molecule^{-2} cm^6 s^{-1} and $(1.2 \pm 0.4) \times 10^{-11}$ molecule^{-1} cm^3 s^{-1}, respectively. The listed uncertainties are $\pm 2\sigma$.

Rh($a^4F_{9/2}$) + N_2

Initial experiments were attempted using nitrogen as the buffer gas; however, further inquiry indicated Rh($a^4F_{9/2}$) slowly reacts with N_2 through a termolecular mechanism. This observation is consistent with a theoretical study reported previously [36]. The room temperature rate constants for the $a^4F_{9/2}$ state were measured at 100, 200 and 300 Torr; the values of the rate constants are 1.1×10^{-14}, 2.0×10^{-14}, and 3.0×10^{-14} molecule^{-1} cm^3 s^{-1}, respectively. These rate constants are essentially linear as a function of total pressure. Assuming linearity

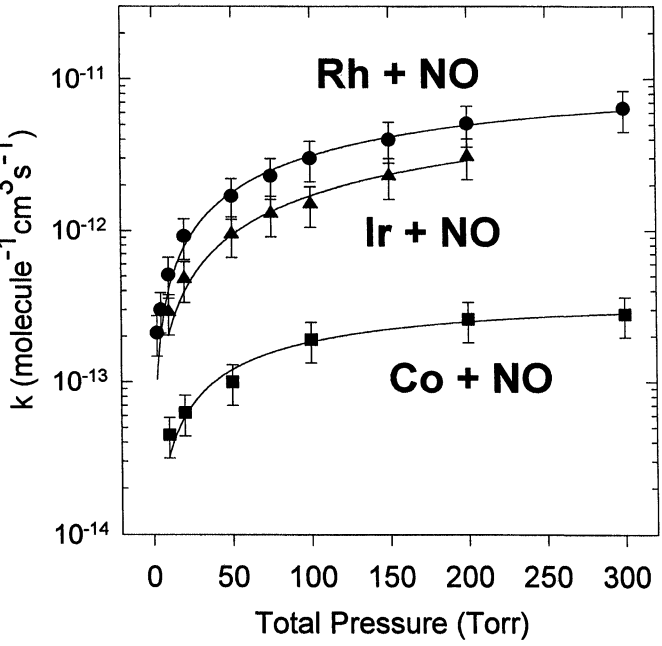

FIGURE 6 Rate constants for the reaction of ground state rhodium, cobalt and iridium + NO at room temperature. Error bars represent ±30% uncertainty. The solid lines are fits to Eq. (4).

down to zero pressure, a value of 3×10^{-33} molecule^{-2}cm^{6}s^{-1} is calculated for the limiting low-pressure third-order rate constant, k_0. The only other transition metal reported to react with N_2 is niobium. The low-pressure third order rate constant reported here for rhodium is a factor of ten smaller than the value reported for niobium [23].

Reactions of Rh*

Bimolecular removal rate constants for the low-lying excited electronic states of rhodium were also measured at 20 Torr and 296 K and are listed in Table III. In the presence of all three oxidants, the low-lying excited electronic states relax/react at a faster rate than the ground state. We are unable to distinguish between physical quenching and chemical reaction in these experiments although the growth in the ground state temporal profiles indicates physical quenching to the

TABLE III Second-order removal rate constants for the low-lying states of rhodium in O_2, N_2O and NO (P_{total} = 20.0 Torr, Ar buffer)

Electronic State	*Electronic Energy* (cm^{-1}) [a]	*Transition Wavelength* (*nm*) [b]	k_{2nd} ($/10^{-12}$ *molecule*$^{-1}$ *cm*^{3} *s*$^{-1}$)			
			O_2	*N_2O*	*NO*	*N_2*
$d^8s^1\,a^4F_{9/2}$	0	369.24	3.6	0.73	0.92	< 0.01
$d^8s^1\,a^4F_{7/2}$	1530	370.09	[c]	[c]	[c]	–
$d^8s^1\,a^4F_{5/2}$	2598	380.68	[d]	[d]	[d]	[d]
$d^9\,a^2D_{5/2}$	3310	369.07	81.0	42.0	87.0	9.9
$d^8s^1\,a^4F_{3/2}$	3473	371.30	20.0	10.0	57.0	0.43
$d^9\,a^2D_{3/2}$	5658	378.85	110.0	61.0	85.0	13.0
$d^8s^1\,a^2F_{7/2}$	5691	379.32	110.0	59.0	77.0	13.0
$d^8s^1\,a^2F_{5/2}$	7791	408.28	83.0	140.0	63.0	2.0
$d^8s^1\,a^4P_{5/2}$	9221	382.85	61.0	1.9	82.0	< 0.01
$d^8s^1\,a^4P_{3/2}$	10313	394.27	60.0	3.4	74.0	0.88
$d^8s^1\,a^4P_{1/2}$	11006	405.34	76.0	4.2	92.0	0.08
$d^8s^1\,a^2P_{3/2}$	11968	497.92	31.0	9.0	93.0	1.0
$d^7s^2\,b^4F_{9/2}$	12723	598.36	10.0	3.1	7.3	0.045

[a] Ref. [38].
[b] Ref. [34].
[c] Exhibited biexponential behavior in the presence of oxidant; the rate constant, however, is large based on reaction time constants of only 2.0, 2.5 and 3.3 μs in 0.38 Torr O_2, N_2O and NO, respectively, for the short time decay.
[d] Although observed, the LIF signal for this state was too weak to measure rate constant values.

ground state does occur. Removal rate constants are included for N_2 for comparison since the *chemical* removal rate in the presence of N_2 is expected to be slow.

DISCUSSION

Rh + N_2O

The bimolecular abstraction reaction of ground state rhodium with N_2O:

$$Rh(a^4F_{9/2}) + N_2O(X^1\Sigma^+) \rightarrow RhO + N_2(X^1\Sigma_g^+) \qquad (5)$$

has an exothermicity of 254 kJ; therefore, there are no thermodynamic barriers for this reaction [37]. Our experimental results for this reaction are consistent with a bimolecular reaction; thus, the most likely reaction channel is reaction (5). In general, abstraction reactions

of TM atoms with N_2O are exothermic due to the formation of the stable N_2 and metal oxide molecules. Despite this exothermicity, TM reactions with N_2O have been observed to have significant energy barriers. The reactivity behavior of rhodium with N_2O is unusual compared to the other TMs studied thus far. The large majority of TM reactions with N_2O show typical Arrhenius behavior. For the TMs studied thus far, the experimentally determined barriers vary over a wide range [24], although the frequency factors are all near the gas-kinetic collision rate. The rate constants of only two transition metals (Ru and Cu) have been observed to exhibit biexponential (*i.e.*, non-Arrhenius) behavior as a function of temperature in the presence of N_2O. Copper's deviation from normal Arrhenius behavior, however, occurs only at very high temperatures ($T > 1200\,K$) [7]. The biexponential behavior of ruthenium occurs at lower temperatures as shown in Figure 4. The biexponential behavior has been attributed to two different reaction pathways, an adiabatic pathway with a frequency factor near the gas-kinetic collision rate and a relatively large barrier (~ 38 kJ/mole) and a second nonadiabatic pathway with a frequency factor approximately 1% of the collision frequency and a smaller barrier (~ 11 kJ/mole). The small frequency factor in the second channel is attributed to the low probability of the reaction making the required nonadiabatic transition to an excited triplet surface [20].

The rate constants observed here for rhodium exhibit almost temperature independence; *i.e.*, the Arrhenius activation energy is very small. In this case, the frequency factor is only about 1% of the gas-kinetic collision rate. Thus, rhodium's behavior is similar to the low temperature behavior exhibited by ruthenium. Thus, the dynamic behavior of rhodium might be similar to ruthenium; however, due to the temperature limitations for the measurement of these rate constants, the second adiabatic pathway with the larger barrier is not seen. The nonadiabatic, low-barrier channel might be the result of the surface resulting from the low-lying $d^9a^2D_{5/2}$ state only $3310\,cm^{-1}$ above the ground state [38]. Calculations involving rhodium reacting with hydrocarbons indicate this state has the smallest repulsion in the entrance channel of all the low-lying states of rhodium [39]. Thus, it is rhodium's low-lying electronic structure which results in its unusual reactivity with nitrous oxide.

A comparison of the rate constants for the reaction of nitrous oxide with Co (the Group 9 metal directly above Rh) indicates rhodium's rate constants are greater than cobalt's by at least three orders of magnitude over the temperature range studied [40]. The rate constants of cobalt exhibit normal Arrhenius behavior (Fig. 4) so only one reaction pathway appears to be operative. The Arrhenius activation energy for cobalt is large so the reaction rate is slow even at elevated temperatures. The reaction of iridium with N_2O is also very slow with an estimated activation energy of at least 45 kJ/mole [29]. If rhodium exhibits a second adiabatic channel with a barrier similar to the other Group 9 atoms, then the biexponential form of the Arrhenius plot would only be seen at temperatures much higher than the temperatures studied here. Thus, experiments performed at higher temperatures are needed to verify this assertion.

Fontijn and co-workers have advanced a resonance interactions model [41–44] to predict barriers to reaction and rate constants for metal atoms reacting with N_2O. In this model, the activation barriers are calculated by taking into account the ionzation potential and sp promotion energy of the metal, the electron affinity of N_2O, and the bond energy of the metal oxide product. The predicting ability of this model for TMs has been limited. The resonance model predicts a barrier of 33 kJ/mole for rhodium [41], a value much larger than the activation energy observed here.

$Rh + O_2$

Results for the reaction of rhodium with O_2 indicate a termolecular reaction mechanism:

$$Rh + O_2 \xrightarrow{[Ar]} RhO_2 \qquad \Delta H^\circ = -394 \text{ kJ/mole [37]} \qquad (6)$$

RhO_2 has been observed previously from the reaction of laser-vaporized rhodium metal with O_2 [45]. The bimolecular abstraction channel to produce RhO is endothermic by 77 kJ/mole [37]; thus, the thermodynamic barrier prohibits this pathway at the temperatures studied here. The value of the limiting low-pressure third-order rate constant is relatively large, consistent with other termolecular reactions with O_2 involving s^1d^{n-1} transition metals. Previous studies

of the 3*d* TM association reactions with O_2 indicate that TMs with ground state or low-lying s^1d^{n-1} configurations are reactive whereas TMs with s^2d^{n-2} ground state configurations are unreactive [6]. This behavior has been explained in terms of simple molecular orbital concepts. In the approach of the TM to O_2, the nature of the potential in the region of the onset of orbital overlap will be determined by the interaction between the *s*-orbital of the TM atom (which has a larger spatial extent than the *d*-orbitals) and the in-plane π^*-antibonding orbital of O_2. For a TM atom with an s^1 configuration, an electron pair bond may be formed from the overlap of these orbitals, as in a radical–radical recombination process. In the case of an s^2 configuration, one of the *s*-electrons occupies the antibonding molecular orbital between the TM atom and O_2, which destabilizes the complex and leads to a less attractive or a repulsive potential [6].

The variation with total pressure of the second-order rate constants at room temperature of the other two Group 9 atoms are included in Figure 5. The termolecular fitting parameters are listed in Table IV. It can be seen that the order of reactivity for this group is Rh > Ir > Co. Since rhodium's ground state electron configuration has a single valence *s* electron ($5s^14d^8$), it is not unexpected that the termolecular reaction with O_2 is faster than the other two Group 9 atoms with s^2d^8 ground state configurations. This order is also consistent with the relative energies of the s^1d^8 excited states in iridium and cobalt. Furthermore, the ordering is also consistent with size considerations of the valence *s* and *d* orbitals. A better size match between the *s* and *d* orbitals might help drive the reaction due to increased incorporation of *d* orbitals in the bonding. The 4*d* series has the best size match,

TABLE IV Termolecular modeling parameters for the reactions of the Group 9 metals with O_2 and NO at room temperature

TM (buffer)	*Reactant*	k_0 ($molecule^{-2}\,cm^6\,s^{-1}$)	k_∞ ($molecule^{-1}\,cm^3\,s^{-1}$)	*Ref.*
Co (Ar)	O_2	$(1.2\pm0.3)\times10^{-31}$	$(7.5\pm0.5)\times10^{-14}$	[47]
Rh (Ar)	O_2	$(6.6\pm0.6)\times10^{-30}$	$(2.1\pm0.2)\times10^{-11}$	this work
Ir (N_2)	O_2	$(4.8\pm1.6)\times10^{-30}$	$(3.6\pm0.4)\times10^{-12}$	[28]
Co (Ar)	NO	$(1.1\pm0.3)\times10^{-31}$	$(3.9\pm1.0)\times10^{-13}$	[47]
Rh (Ar)	NO	$(1.3\pm0.2)\times10^{-30}$	$(1.2\pm0.4)\times10^{-11}$	this work
Ir (N_2)	NO	$(6.3\pm1.5)\times10^{-31}$	$(9.8\pm0.8)\times10^{-12}$	[47]

followed by the $5d$ series. The difference in size between the $3d$ and $4s$ orbitals in the $3d$ series appears to be make these reactions particularly inefficient for atoms with s^2d^{n-2} ground states. A more thorough quantitative understanding of the dynamics of these reactions awaits accurate theoretical calculations.

Rh + NO

Results of the reaction of $Rh(a^4F_{9/2}) + NO$ indicate a termolecular reaction mechanism.

$$Rh + NO \xrightarrow{[Ar]} RhNO \tag{7}$$

Production of RhO from the abstraction channel is endothermic by 211 kJ/mole [37].

Termolecular processes are expected for the majority of TM atoms reacting with NO since only the Group 3, 4, 5 atoms along with tungsten have exothermic abstraction reactions with NO. Thus far, extensive pressure-dependent rate constants have been determined for chromium [5], iron [4, 46], cobalt [47], manganese [46], molybdenum [19], ruthenium [46], rhenium [30], iridium [47] and platinum [29]. The three atoms in the $3d$ series with s^2d^{n-2} electron configurations are extremely inefficient processes with NO whereas the TMs with s^1d^{n-1} configurations have much more efficient reactions. In the s^1 configuration, the singly occupied orbital of the TM might overlap favorably with the unpaired electron on NO, forming a bond. This argument is the same rational used to explain the reactivity dependence on electron configuration in the termolecular reactions of $3d$ TM atoms with O_2. Even if the d electrons of the TM atom are involved in the bonding, the reactivity of the s^2 configuration would still be expected to be less than that of the s^1 configuration because of its more diffuse nature. The rate constants for rhenium and iridium of the $5d$ series are much more efficient than the atoms with s^2d^{n-2} in the $3d$ series. These reactivity differences might again be explained by the better size match of the s and d orbitals of the $5d$ series compared to the $3d$ series.

The variation with total pressure of the second-order rate constants at room temperature of the other two Group 9 atoms are included in Figure 6. The termolecular fitting parameters are listed in Table IV.

Again, it can be seen that the order of reactivity with NO for this group is Rh > Ir > Co. The same arguments used to explain the reactivity order with O_2 also apply to the reaction with NO.

SUMMARY

We have measured the rate constants as a function of temperature and pressure for the reaction of ground state rhodium ($a^4F_{9/2}$) with N_2O, O_2 and NO. The reaction of rhodium with N_2O has been shown to be a bimolecular reaction. The reaction is slow although the activation energy is small. The inefficiency of the reaction is attributed to the low probability of a surface hopping to the reactive surface as the reactants approach. The relatively small A factor for the production of RhO indicates the low probability for the non-adiabatic transition. The reaction of ground state rhodium with both oxygen and nitric oxide involve termolecular processes. The reaction is rapid compared to other termolecular reactions involving transition metals. The rapidity of the reaction is attributed to the s^1d^{n-1} electron configuration of rhodium.

Acknowledgements

Acknowledgment is made to the Donors of the Petroleum Research Fund, administered by the American Chemical Society, for partial support of this research. This research was supported by a Cottrell College Science Award of Research Corporation.

References

[1] Vinckier, C., Corthouts, J. and DeJaegere, S. (1988). *J. Chem. Soc., Faraday Trans. 2*, **84**, 1951.
[2] Ritter, D. and Weisshaar, J. C. (1989). *J. Phys. Chem.*, **93**, 1576.
[3] Ritter, D. and Weisshaar, J. C. (1990). *J. Phys. Chem.*, **94**, 4907.
[4] Mitchell, S. A. and Hackett, P. A. (1990). *J. Chem. Phys.*, **93**, 7822.
[5] Parnis, J. M., Mitchell, S. A. and Hackett, P. A. (1990). *J. Phys. Chem.*, **94**, 8152.
[6] Brown, C. E., Mitchell, S. A. and Hackett, P. A. (1991). *J. Chem. Phys.*, **95**, 1062.
[7] Narayan, A. S., Futerko, P. M. and Fontijn, A. (1992). *J. Chem. Phys.*, **96**, 290.
[8] McClean, R. E. and Pasternack, L. (1992). *J. Phys. Chem.*, **96**, 9828.
[9] Campbell, M. L. and McClean, R. E. (1993). *J. Phys. Chem.*, **97**, 7942.

[10] Clemmer, D. E., Honma, K. and Koyano, I. (1993). *J. Phys. Chem.*, **97**, 11480.
[11] Helmer, M. and Plane, J. M. C. (1994). *J. Chem. Soc., Faraday Trans.*, **90**, 31.
[12] Helmer, M. and Plane, J. M. C. (1994). *J. Chem Soc., Faraday Trans.*, **90**, 395.
[13] Fontijn, A., Blue, A. S., Narayan, A. S. and Bajaj, P. N. (1994). *Combust. Sci. and Tech.*, **101**, 59.
[14] Lian, L., Mitchell, S. A. and Rayner, D. M. (1994). *J. Phys. Chem.*, **98**, 11637.
[15] Campbell, M. L., McClean, R. E. and Harter, J. S. S. (1995). *Chem. Phys. Lett.*, **235**, 497.
[16] Campbell, M. L. and McClean, R. E. (1995). *J. Chem. Soc., Faraday Trans.*, **91**, 3787.
[17] Campbell, M. L. and Metzger, J. R. (1996). *Chem. Phys. Lett.*, **253**, 158.
[18] Campbell, M. L. (1996). *J. Chem. Phys.*, **104**, 7515.
[19] McClean, R. E., Campbell, M. L. and Goodwin, R. H. (1996). *J. Phys. Chem.*, **100**, 7502.
[20] Campbell, M. L. (1996). *J. Chem. Soc., Faraday Trans.*, **92**, 4377.
[21] Matsui, R., Senba, K. and Honma, K. (1996). *Chem. Phys. Lett.*, **250**, 560.
[22] Campbell, M. L. (1996). *J. Phys. Chem.*, **100**, 19430.
[23] McClean, R. E, Campbell, M. L. and Kölsch, E. J. (1997). *J. Phys. Chem. A*, **101**, 3348.
[24] Campbell, M. L., Hooper, K. L. and Kölsch, E. J. (1997). *Chem. Phys. Lett.*, **274**, 7.
[25] Matsui, R., Senba, K. and Honma, K. (1997). *J. Phys. Chem. A*, **101**, 179.
[26] Harter, J. S. S., Campbell, M. L. and McClean, R. E. (1997). *Int. J. Chem. Kinet.*, **29**, 367.
[27] Campbell, M. L. and Hooper, K. L. (1997). *J. Chem. Soc., Faraday Trans.*, **93**, 2139.
[28] Campbell, M. L. (1997). *J. Phys. Chem. A*, **101**, 9377.
[29] Campbell, M. L. (1998). *J. Chem. Soc., Faraday Trans.*, **94**, 353.
[30] Campbell, M. L. (1998). *J. Phys. Chem. A*, **102**, 892.
[31] Carroll, J. J., Haug, K. L., Weisshaar, J. C., Blomberg, M. R. A., Siegbahn, P. E. M. and Svensson, M. (1995). *J. Phys. Chem.*, **99**, 13955.
[32] Campbell, M. L. (1997). *J. Am. Chem. Soc.*, **119**, 5984.
[33] (a) Salanov, A. N. and Savchenko, V. I. (1993). *Kinetics and Catalysis*, **34**, 478; (b) Zhu, G. X., Cao, P., Jiang, Q. Z. and Zhang, X. M. (1997). *J. Am. Chem. Soc.*, **119**, 1799; (c) Wong, J. C. S. and Yates, J. T. (1995). *J. Phys. Chem.*, **99**, 12640; (d) Bond, G. C., Calhoun, J. and Hooper, A. D. (1996). *J. Chem. Soc., Faraday Trans.*, **92**, 5117; (e) Araya, P. and Cortes, J. (1997). *J. Chem. Soc., Faraday Trans.*, **93**, 639; (f) Vanhardeveld, R. M., Vansanten, R. A. and Niemantsverdriet, J. W. (1997). *J. Phys. Chem. B*, **101**, 998.
[34] Duquette, D. W. and Lawler, J. E. (1985). *J. Opt. Soc. Am. B*, **2**, 1948.
[35] Robinson, P. J. and Holbrook, K. A. (1972). Unimolecular Reactions, Wiley-Interscience: New York.
[36] McKee, M. L. and Worley, S. D. (1997). *J. Phys. Chem. A*, **101**, 5600.
[37] Wagman, D. D., Evans, W. H., Parker, V. B., Schumm, R. H., Halow, I., Bailey, S. M., Churney, K. L. and Nuttall, R. L. (1982). The NBS tables of chemical thermodynamic properties, *J. Phys. Chem. Ref. Data*, **11**, Suppl. 2.
[38] Moore, C. E. (1971). NBS Circular 467; U.S. Department of Commerce: Washington DC, Vol. III.
[39] Blomberg, M. R. A., Siegbahn, P. E. M. and Svensson, M. (1992). *J. Amer. Chem. Soc.*, **114**, 6095.
[40] (a) Kölsch, E. J. (1997). Trident Scholar Project Report No. 249; USNA Printing Office: Annapolis, MD; (b) Campbell, M. L., Kölsch, E. J. and Hooper, K. L., manuscript in preparation.
[41] Futerko, P. M. and Fontijn, A. (1991). *J. Chem. Phys.*, **95**, 8065.
[42] Futerko, P. M. and Fontijn, A. (1992). *J. Chem. Phys.*, **97**, 3861.

[43] Futerko, P. M. and Fontijn, A. (1993). *J. Chem. Phys.*, **98**, 7004.
[44] Belyung, D. P., Futerko, P. M. and Fontijn, A. (1995). *J. Chem. Phys.*, **102**, 155.
[45] Van Zee, R. J., Hamrick, Y. M., Li, S. and Weltner, W. Jr. (1992). *J. Phys. Chem.*, **96**, 7247.
[46] McClean, R. E., Campbell, M. L., Vorce, M. D. and Medhurst, L. J., *J. Phys. Chem.*, submitted.
[47] McClean, R. E. and Campbell, M. L., unpublished results.